Soft Matter

PAPER

View Article Online
View Journal | View Issue



Cite this: *Soft Matter*, 2024, **20**, 1320

# Rheological behavior of Pluronic/Pluronic diacrylate hydrogels used for bacteria encapsulation in engineered living materials†

Shardul Bhusari,[ab] Maxi Hoffmann,[c] Petra Herbeck-Engel,[a] Shrikrishnan Sankaran,[a] Manfred Wilhelm[c] and Aránzazu del Campo *[ab]

Received 24th August 2023,
Accepted 6th December 2023

DOI: 10.1039/d3sm01119d

rsc.li/soft-matter-journal

Pluronic (Plu) hydrogels mixed with variable fractions of Pluronic diacrylate (PluDA) have become popular matrices to encapsulate bacteria and control their growth in engineered living materials. Here we study the rheological response of 30 wt% Plu/PluDA hydrogels with PluDA fraction between 0 and 1. We quantify the range of viscoelastic properties that can be covered in this system by varying in the PluDA fraction. We present stress relaxation and creep-recovery experiments and describe the variation of the critical yield strain/stress, relaxation and recovery parameters of Plu/PluDA hydrogels as function of the covalent crosslinking degree using the Burgers and Weilbull models. The analyzed hydrogels present two stress relaxations with different timescales which can be tuned with the covalent crosslinking degree. We expect this study to help users of Plu/PluDA hydrogels to estimate the mechanical properties of their systems, and to correlate them with the behaviour of bacteria in future Plu/PluDA devices of similar composition.



## 1. Introduction

Soft hydrogel networks with combined physical (dynamic) and covalent (permanent) crosslinks are interesting materials for the encapsulation and controlled expansion of cells.[1,2] The inherent reorganization capability of the dynamic crosslinks allows cells to deform the surrounding material as they proliferate and accommodate daughter cells. In parallel, the elasticity of the network imposes an increasing compressive force on the cell population as it grows and controls its size.[3,4] Hydrogels formed by mixtures of Pluronic ($PEO_x$-$PPO_y$-$PEO_x$) and Pluronic diacrylate have been successfully used to embed and regulate the growth of bacteria and yeast in engineered living materials.[1,5–9] Despite the application potential of the developed systems, a systematic analysis of the mechanical properties of these hydrogels is still missing.

Physical Pluronic hydrogels are formed by aggregation of the Pluronic micelles into clusters through the interactions between the PEO coronas (Scheme 1). Above the transition temperature, the micellar clusters grow and build a 3D network.[10,11] For the specific Pluronic F127 ($PEO_{106}$-$PPO_{70}$-$PEO_{106}$), frequently used in bacteria encapsulation and also for the experiments in this article, the critical micellar concentration (cmc) is at 0.725 wt% in water at 25 °C,[12–14] and the sol–gel transition occurs at polymer concentrations >5 wt% and temperatures above 14 °C. The assembly of Pluronic F127 chains in 3D networks has been studied by scattering methods like dynamic light scattering (DLS) and small angle neutron scattering (SANS).[14,15] The order of the micelles in the clusters depends on external conditions (*i.e.*, temperature, salt concentration, shear forces)[15,16] and ranges from perfect face-centered cubic (FCC) or hexagonally close packed (HCP) structures to random stackings. As associative physical networks, Pluronic hydrogels show elastic properties in the quiescent state and undergo yielding, *i.e.* fracture and flow, when the stress surpasses the interparticle forces.[17,18] The shear thinning behavior and the thermosensitivity makes Pluronic gels interesting from a biomedical perspective.[19] It allows them to be easily mixed with cells or other payloads and processed using shear forces.[20–22]

Physical Pluronic (Plu) hydrogels swell and dissociate into individual micelles when immersed in water. The introduction of polymerizable acrylate functionalities as end-groups of the Pluronic chains provides the possibility to stabilize the micellar hydrogel *via* the formation of permanent, covalent bonds between the micelles.[7,11] Covalent crosslinking affects the mechanical behavior, specially the elasticity as quantified *via* $G'$ of the hydrogel.[1] By varying the Pluronic diacrylate (PluDA)

[a] *INM-Leibniz Institute for New Materials, Campus D2 2, 66123 Saarbrücken, Germany. E-mail: aranzazu.delcampo@leibniz-inm.de*
[b] *Chemistry Department, Saarland University, 66123 Saarbrücken, Germany*
[c] *Karlsruhe Institute of Technology (KIT), Institute for Chemical Technology and Polymer Chemistry (ITCP), Engesserstraße 18, 76131 Karlsruhe, Germany*

† Electronic supplementary information (ESI) available. See DOI: https://doi.org/10.1039/d3sm01119d

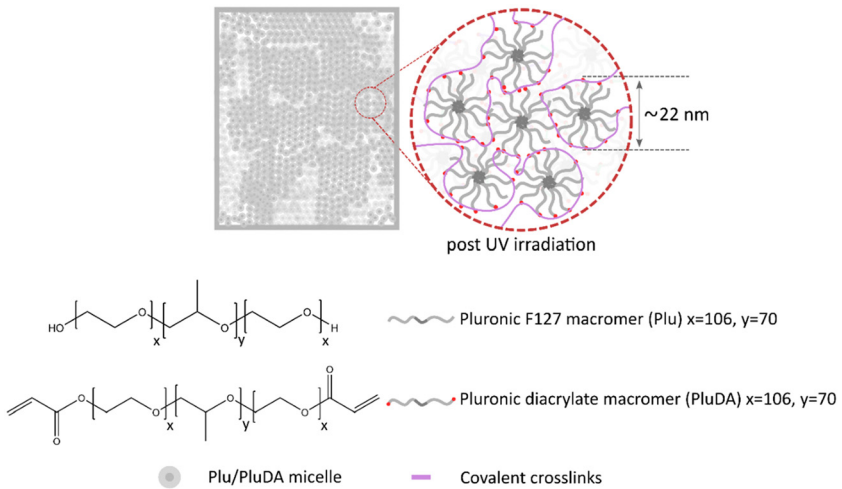


Scheme 1 Micellar structure of the Plu/PluDA hydrogel representing the organization of the $PEO_x$-$PPO_y$-$PEO_x$ triblock copolymer chains above the sol–gel transition temperature. The micelles have a diameter of *ca.* 22 nm and build aggregates that form a network with the inter- and intra-micellar covalent crosslinks between PluDA chains.

fraction in Plu/PluDA hydrogels the density of chemical crosslinks in the hydrogel and the resulting mechanical properties can be tuned. For example, 30 wt% Plu/PluDA hydrogels show increasing elastic responses ($G'$) from 17.8 ± 1.4 to 42.9 ± 1.9 kPa and decreasing non-elastic responses (from creep-recovery curves) when the PluDA fraction in the mixture increased from 0 to 100%.[1]

Here we present a detailed study of the time-dependent rheological behavior of Plu/PluDA hydrogels as a function of PluDA fraction. We use 30 wt% Plu/PluDA hydrogels as used in preceding reports for the fabrication of engineered living materials by different groups.[6,7,23,24]

## 2. Materials and methods

### 2.1. Sample preparation

Pluronic diacrylate (PluDA) was synthesized by reaction of Pluronic F127 (Plu) with acryloyl chloride in the presence of triethylamine according to a reported protocol.[11] Acrylation degrees of 70% were typically obtained.

Plu/PluDA hydrogels were prepared by mixing stock solutions of Plu and PluDA polymers as previously reported.[1] The resulting hydrogels were named DA *X*, with *X* being the fraction of PluDA in the Plu/PluDA mixture, between 0 and 100%. 30 wt% Plu and PluDA stock solutions (named DA0 and DA100, respectively) were prepared in milliQ water (300 mg polymer in 1 mL water) and contained 0.2% w/v Irgacure 2959 (Sigma-Aldrich Co.) as photoinitiator. Solutions were stored at 4 °C. DA 25, DA 50 and DA 75 hydrogels were prepared by mixing DA 0 and DA 100 stock solutions in the following ratios- 3 : 1 (DA 25), 1 : 1 (DA 50) and 1 : 3 (DA 75). After mixing, the DA *X* hydrogels were allowed to form at room temperature for 10 minutes.[25] For the photoinitiated crosslinking, hydrogels were exposed to UV light (365 nm, 6 mW $cm^{-2}$) using a OmniCure Series 1500 lamp for 60 s through a UV transparent bottom plate for rheology.

### 2.2. Raman spectroscopy of Plu/PluDA powders and DA 0–100 hydrogels

Raman investigations were carried out at ambient conditions on a LabRAM HR Evolution HORIBA Jobin Yvon A Raman microscope (Longmujeau, France) using a 633 nm He–Ne laser (Melles Griot, IDEX Optics and Photonics, Albuquerque, NM, USA) equipped with 1800 lines per 1 mm grating.

### 2.3. Rheological measurements

The rheological properties were measured with a stress-controlled rheometer (DHR 3, TA Instruments) using a parallel plate geometry. A 20 mm Peltier plate/UV transparent plate was used as bottom plate and a smooth stainless steel 12 mm disk was used as top plate. The rheometer was equipped with a UV Source (OmniCure, Series 1500, 365 nm, 6 mW $cm^{-2}$) for illumination of the hydrogel samples in between the rheometer plates. Experiments were performed at room temperature (22–23 °C). To avoid drying of the sample by evaporation during testing a solvent trap was used and the sample was sealed with silicone oil.

The 30 wt% DA *X* hydrogels were prepared by pipetting 35 μL of freshly prepared 30 wt% DA *X* precursor solutions on the rheometer plate, and allowing the gel to form between the plates (diameter 12 mm, gap 300 μm) during 10 min. The polymerization of the acrylate groups was initiated by exposure to 365 nm (6 mW $cm^{-2}$) through the UV transparent bottom plate. Strain sweeps were conducted from 0.001% to 1000% at a frequency of 1 Hz. In the strain amplitude sweep curves, a line was fit to the plateau region (linear) and the drop-off region (non-linear). The intersection was taken as the critical strain value ($\gamma_y$).[26,27] Fluidization strain ($\gamma_F$) was taken as the value at the intersection of $G'$ and $G''$, *i.e.*, at $G' = G''$.[27] The corresponding stress values were used as critical stress ($\tau_y$) and fluidization stress ($\tau_F$) values. The experimental conditions for the rheological experiments were taken from our previous work.[1]

### 2.4. Stress relaxation measurements

In the stress relaxation experiment, strains of 0.5, 1, 2, 5, 10, 15 and 30% were applied to the same sample (DA 0, 50 and 100, $n$ = 3) for 300 s with a strain raise time of 0.2 s. To avoid cumulative stress buildup and shear history effects, the strain was reversed (negative strain, equivalent to the positive strain) after each run to reach rheometer stress = 0 Pa, and the next run was started after 10 min equilibration time.

In another experiment, a constant strain of 1% was applied to the sample (strain raise time 0.01 s) and the stress was monitored for 300 s. Each experiment was repeated three times.

The percentage of relaxation was defined as the drop in the relaxation modulus from the start (30 ms) to the end (300 s) of the experiment normalized by the starting relaxation modulus.[28]

The relaxation curves were fitted to a linear combination of two stretched exponential or Kohlrausch–Williams–Watts (KWW) functions,[29]

$$G = G_0\left\{\left(A \times \exp\left[-\left(\frac{t}{\tau_1}\right)^{\beta_1}\right]\right) + (1-A) \times \exp\left[-\left(\frac{t}{\tau_2}\right)^{\beta_2}\right]\right\} + G_e \quad (1)$$

where $G_0$ is the relaxation modulus linearly extrapolated to zero time, $\tau_1$ and $\tau_2$ are the viscoelastic relaxation times for the two processes ($0 < \tau$), $\beta_1$ and $\beta_2$ are stretching exponents for the two processes ($0 < \beta \leq 1$) that reflect the width of the relaxation time distribution. The parameter $A$ is the fractional contribution of the fast relaxation to the whole relaxation process ($0 < A$) and $G_e$ is the equilibrium relaxation shear modulus.

### 2.5. Creep recovery measurements

A shear stress of 100 Pa was applied for 180 s to the hydrogel sample in the rheometer. The shear strain was monitored during this time (creep phase), and for a further 180 s after removal of the shear stress (recovery phase). Creep ringing phenomenon was observed at short time scales (2 s) in the creep and recovery experiments.[28]

Creep deformation, $\gamma_{creep}$, was fitted to a four parameter Burgers model:[30–32]

$$\gamma_{creep} = \frac{\tau}{G_m} + \frac{\tau}{G_k}\left(1 - \exp^{\frac{-t}{\lambda}}\right) + \frac{\tau}{\eta_m}t \quad (2)$$

where $\tau$ is the applied shear stress (100 Pa), t denotes the time after loading, $G_m$ denotes the shear modulus (or spring constant) of the spring, $\eta_m$ denotes the viscosity of the dashpot in the Maxwell element, $G_k$ denotes the shear modulus (or spring constant) and $\eta_k$ denotes the viscosity of the dashpot in the Kelvin element, and $\lambda$ is the retardation time ($\eta_k/G_k$) needed to achieve 63.2% of the total deformation in the Kelvin unit. The non-linear curve fit function of the OriginPro 9.1 software was used for the fitting and four parameters ($G_m$, $G_k$, $\eta_m$ and $\tau$) were defined. Creep ringing phenomenon was observed at short time scales. Therefore only data at $t > 2$ s were considered in the fitting process.[28]

Recovery data was fitted to a Weibull distribution function.[30,33]

$$\gamma_{rec} = \gamma_k\left\{\exp\left[-\left(\frac{t-t_0}{\eta_r}\right)^{\beta}\right]\right\} + \gamma_p \quad (3)$$

where where $\gamma_{rec}$ denotes the deformation after the instantaneous strain recovery, $\gamma_k$ denotes the delayed viscoelastic strain recovery (Kelvin–Voigt element), $\eta_r$ is the characteristic life parameter, $t$ is the induction time and $\beta$ the shape factor. The stress is removed at time $t_0$ (180 s) and $\gamma_p$ is the permanent irreversible strain. Ringing phenomenon was observed again at short time scales as in creep data. Therefore, $t_0$ = 182 s was considered for the fitting.

### 2.6. Statistical analyses

Non-linear curve fit function of the OriginPro 9.1 software was used for the fitting of the rheological curves. Concrete parameters used for the different types of analyses performed have been described in the sections and figure captions of the related experiments.

## 3. Results

Plu/PluDA hydrogels were prepared from mixtures of defined volumes of 30 wt% solutions of Plu and PluDA polymers in water.[1] The hydrogels were named DA $X$, with $X$ being the fraction of PluDA in the Plu/PluDA mixture, between 0 and 100% (Table 1).

### 3.1. Rheological behavior of physical DA 0 and DA 100 hydrogels

A 30 wt% solution of Pluronic F127 (DA 0) in water forms physical hydrogels at temperature >15.5 °C.[1] At room temperature (22 °C) and shear strain amplitudes ($\gamma_0$) below 1%, the DA 0 hydrogel behaves as a linear response viscoelastic solid (Fig. 1a) with a strain amplitude independent shear modulus $G'$ of 15.3 ± 1.6 kPa (Fig. 1b) at $\omega/2\pi$ = 1 Hz. At higher strain amplitudes ($\gamma_0 > 1\%$), DA 0 hydrogels show strain-induced yielding and gradual fluidization (Fig. 1a). This behavior is characteristic of colloidal or granular hydrogels,[34] in which particles aggregate through reversible interparticle interactions to form an interconnected, percolated 3D network structure that yields when the applied stress exceeds the interparticle attractive forces.[26] The critical strain for yielding mainly depends on the particle content and the strength of the interparticle interactions including interparticle (electrostatic, hydrogen bonding, van der Waals, steric, depletion *etc.*) and hydrodynamic forces.[35]

The 30 wt% solutions of diacrylated Pluronic F127 (DA100, 70% end-group functionalization) also form physical hydrogels at a slightly lower temperature of 14 °C.[1] The substitution of the terminal –OH groups by less polar acrylic functionalities in the outer surface of the PEO shell of Pluronic micelles enhances micellar aggregation and gel formation.[11] The resulting

 

Table 1 Composition and mechanical parameters of DA *X* hydrogels. Note that the end-group functionalization degree of PluDA component is 70% and, therefore, the real fraction of covalent fixed chains differs for each composition and reaches 70% as maximum value in DA 100

| Hydrogel name (DA *X*) | Plu:PluDA ratio (mol%) | Ratio of diacrylated endgroups[a] (%) | Shear storage modulus[b] $G'$ (kPa) | Strain amplitude at yield point[b] $\gamma_y$ (%) | Strain amplitude at fluidization[b] $\gamma_F$ (%) | Critical stress[c] $\tau_y$ (kPa) | Fluidization stress[d] $\tau_F$ (kPa) |
|---|---|---|---|---|---|---|---|
| DA 0 | 100 : 0 | 0 | 15.3 ± 1.9 | 1.8 ± 0.6 | 5.5 ± 1.3 | 0.2 ± 0.0 | 0.2 ± 0.0 |
| DA 25 | 75 : 25 | 17.5 | 21.2 ± 2.1 | 6.0 ± 0.4 | 24.1 ± 2.8 | 0.9 ± 0.0 | 1.7 ± 0.0 |
| DA 50 | 50 : 50 | 35 | 25.1 ± 4.2 | 9.5 ± 1.2 | 46.4 ± 7.3 | 1.7 ± 0.3 | 3.9 ± 0.2 |
| DA 75 | 25 : 75 | 52.5 | 37.1 ± 0.7 | 22.8 ± 6.9 | 61.1 ± 21.4 | 5.2 ± 0.8 | 6.7 ± 0.6 |
| DA 100 | 0 : 100 | 70 | 47.5 ± 2.9 | 30.0 ± 14.7 | 65.0 ± 31.3 | 8.3 ± 3.1 | 9.9 ± 0.9 |

[a] Calculated taking into account 70% end-group functionalization of PluDA. [b] From strain amplitude sweep, values at $\gamma_0$ = 0.1% and frequency = 1 Hz (Fig. 1a). [c] Corresponding stress values of $\gamma_y$. [d] Corresponding stress values of $\gamma_F$.

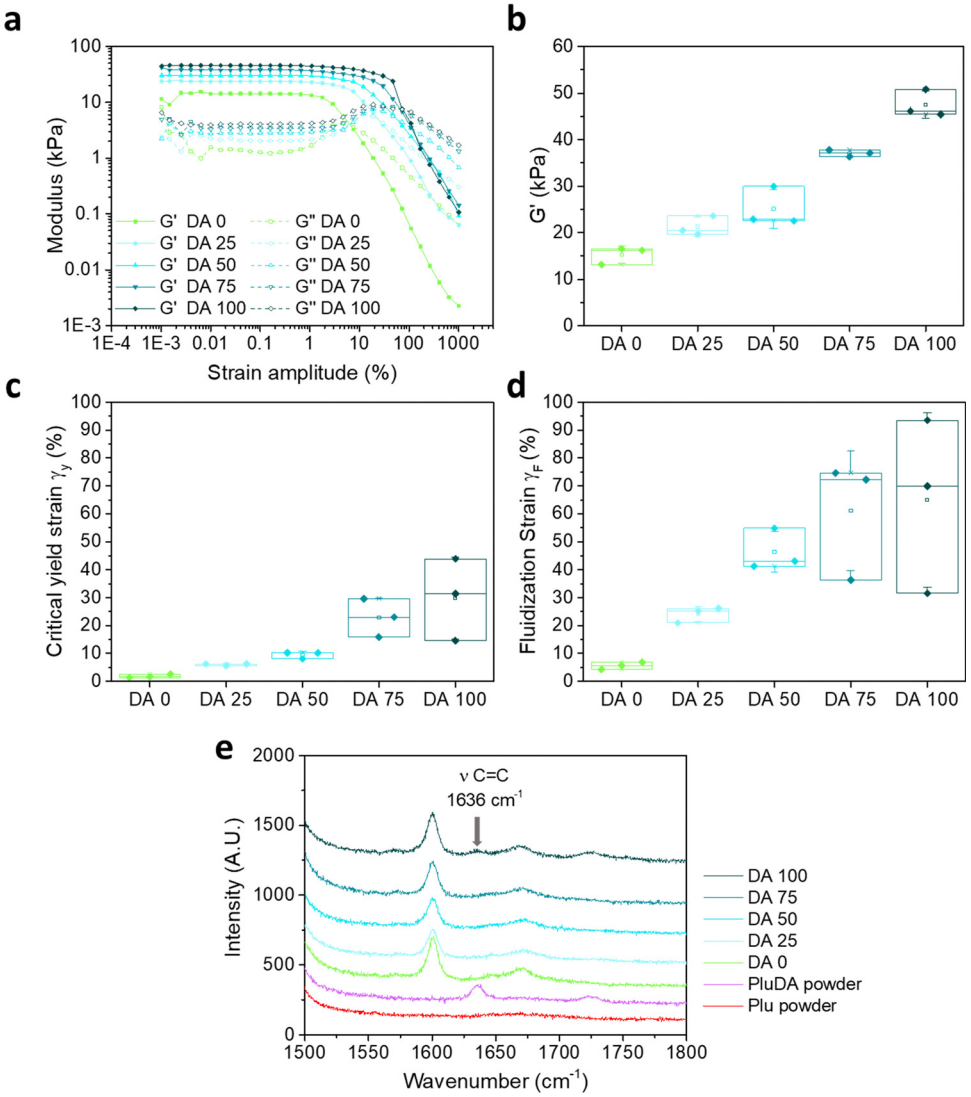


Fig. 1 (a) Representative strain amplitude sweeps of DA *X* hydrogels measured at a frequency of 1 Hz; (b) $G'$ values of DA *X* hydrogels from (a) at 0.1% strain amplitude at a frequency of 1 Hz; (c) values of strain amplitude at critical yield point, $\gamma_y$, and (d) strain amplitude at fluidization point, $\gamma_F$, of DA *X* hydrogels as function of *X* obtained from the strain amplitude sweep experiment in (a), ($N$ = 3, box represents 25 and 75 percentile values and whiskers indicate standard deviation); (e) Raman spectra (vertically shifted for clarity) of Plu and PluDA powders and DA *X* hydrogels. PluDA powder shows the C=C stretching mode ($\nu$) at 1636 cm$^{-1}$. The band at 1600 cm$^{-1}$ in DA *X* hdyrogels corresponds to the –OH bending mode of water molecules, which is absent in Plu and PluDA powders.

physical DA 100 hydrogel shows a similar $G'$ in the linear viscoelastic region (Fig. S1a, ESI†) and a two-fold higher critical strain amplitude for yielding in the strain sweep experiment (Fig. S1b, ESI†) compared to the DA 0 hydrogel, confirming

stronger inter-micellar interactions in the gels with acrylate end-groups.

The strain-sweep curves of the physical DA 0 and DA 100 hydrogels show an overshoot in $G''$ at intermediate strain amplitudes between the linear viscoelastic and the fluidization regions. This overshoot is referred to as the Payne effect and is related to yielding as a gradual transition that occurs while the deformation increases.[36] Strain-dependent breakdown of the internal structure, length scale-dependent rearrangements or forced stress relaxation are believed to contribute to the overshoot of $G''$ as a function of applied strain amplitude.[36]

### 3.2. Rheological behavior of physically *vs.* physically and covalently crosslinked DA 100 hydrogel

Covalently crosslinked DA 100 hydrogels were prepared from 30 wt% PluDA solutions containing 0.2 wt% Irgacure 2959. The solution was left to form a physical gel between the rheometer plates, and it was covalently crosslinked subsequently by exposure to 365 nm light through the UV transparent bottom plate. The degree of conversion of the acrylate groups after polymerization was evaluated by Raman spectroscopy. The characteristic band for the stretching of the C=C bond, observed at 1635 $cm^{-1}$ in the spectrum of PluDA powder, diminished in Plu powder and in the DA 100 hydrogel after UV irradiation (Fig. 1e). This indicates nearly full conversion of the acrylate groups in the photo-crosslinking step.

The polymerization of the acrylate groups influenced the rheological response of the DA 100 hydrogel. The covalently crosslinked hydrogel showed a broader linear viscoelastic range than the exclusively physically crosslinked DA 100, with strain amplitude independent moduli up to $\gamma_0 = 10\%$ (Fig. S1a, ESI†). At higher strain amplitudes, a continuous drop in $G'$ was observed. This strain induced yielding and gradual fluidization suggests that the micellar network in the covalently crosslinked DA 100 hydrogel can undergo major reorganization and stress dissipation and stress release in spite of 70% of the endgroups of the polymeric chains being covalently crosslinked. This behavior can be understood considering that acrylate groups at the PluDA chain terminals can form inter- and intra-micellar crosslinks during the photoinduced polymerization reaction.[11] Micellar clusters which are covalently crosslinked are expected to contribute to the elasticity of the hydrogel and be the reason for the higher $G'$ and higher critical yielding strain of the covalently crosslinked DA 100 hydrogel compared to the physically crosslinked DA 100 hydrogel ($30 \pm 14.7$ *vs.* $4.2 \pm 0.8\%$, Fig. 1c and Fig. S1b, ESI†). Intra-micellar crosslinks stabilize the micelles and form loops in the chains. These crosslinks do not interfere with the inherent ability of physical micellar aggregates to flow above the critical strain. Note that the average residence time of a Pluronic molecule in a physical micellar aggregate has been estimated to be several hours.[37] Therefore, crosslinking during photopolymerization (1 min time scale) can mainly occur between chain ends located in close proximity. The observed strain-induced yielding and fluidization (Fig. 1d) above a critical yield stress in our DA 100 hydrogels suggests that a significant fraction of the covalent crosslinks are intra-micellar. This has been previously suggested by other authors based on gel permeation chromatography (GPC) and light scattering analysis of the sol phase after crosslinking and cooling below the transition temperature.[11]

### 3.3. Rheological behavior of covalently crosslinked DA *X* hydrogels with variable PluDA content

We analysed the rheological response of DA *X* covalent hydrogels as a function of the degree of covalent crosslinking. Near full conversion after the photo-crosslinking step was confirmed by Raman spectroscopy (Fig. 1e).

Covalently crosslinked DA *X* hydrogels showed an increasing trend of $G'$, $\gamma_y$ and $\gamma_F$ values from DA 0 to DA 100 hydrogels. The strain amplitude sweeps showed both a linear viscoelastic and a fluidization region. The storage modulus $G'$ at 0.1% strain amplitude increased from $15.3 \pm 1.8$ to $47.5 \pm 2.9$ kPa as the PluDA content increased from 0 to 100% (Fig. 1c). The critical strain for yielding at 1 Hz, $\gamma_y$, also increased from $1.7 \pm 0.4$ to $29.7 \pm 15.2\%$ (Fig. 1d and Table 1) from DA 0 to DA 100. The strain amplitude needed to reach the fluidization point (crossover of $G''$ and $G'$, as opposite to gelation point), $\gamma_F$, increased from $5.5 \pm 1.2$ to $65.0 \pm 31.3\%$ (Fig. 1e) and the corresponding stress values at the fluidization point ranged from $0.2 \pm 0.0$ to $9.9 \pm 0.9$ kPa (Fig. S2 and Table 1, ESI†). The increase in the density of covalent links between neighboring micelles (inter-micellar) with increasing *X* hinders the viscous deformation of the hydrogel and provides higher mechanical stability and elasticity under the applied strain.

### 3.4. Stress relaxation of DA *X* hydrogels

Fig. 2a–c shows the stress induced in DA 0, DA 50 and DA 100 hydrogels during a stress relaxation experiment with step-strain increase from 0.5 to 30% (300 s) and strain raise time of 200 ms. The stress relaxation curves normalized by the maximum stress values attained during the 200 ms strain raise are also shown. In physical DA 0 hydrogels, the maximum induced stress increased from $78 \pm 17$ to $231 \pm 55$ Pa with increasing applied strain from 0.5 to 5%, and it plateaued for larger shear deformations (Fig. 2d). In contrast, the maximum induced stress in covalently crosslinked DA 100 increased linearly with the strain up to 15% and reached values up to $5708 \pm 246$ Pa (Fig. 2d), denoting a primarily elastic behavior within this strain range. DA 50 showed an intermediate behavior. These differences are in agreement with the observations from the strain sweep experiment (Fig. 1c), where $\gamma_y$ of physical DA 0 hydrogel was $1.8 \pm 0.6\%$ while that for covalently crosslinked DA 100 hydrogel was $30.0 \pm 14.7\%$.

The strain-dependent stress relaxation curves of DA *X* hydrogels were also dependent on the amount of *X* (Fig. 2a). Whereas DA 0 was able to relax the induced step shear stress almost completely within 300 s at all strain values, DA 100 retained at least 60% of the stress, in agreement with its elastic nature (Fig. 2e). DA 50 showed an intermediate behavior with up to 50% relaxation for shear strains $<2\%$, whereas it relaxed $>70\%$ for larger strain values. For all hydrogels, the step shear

 

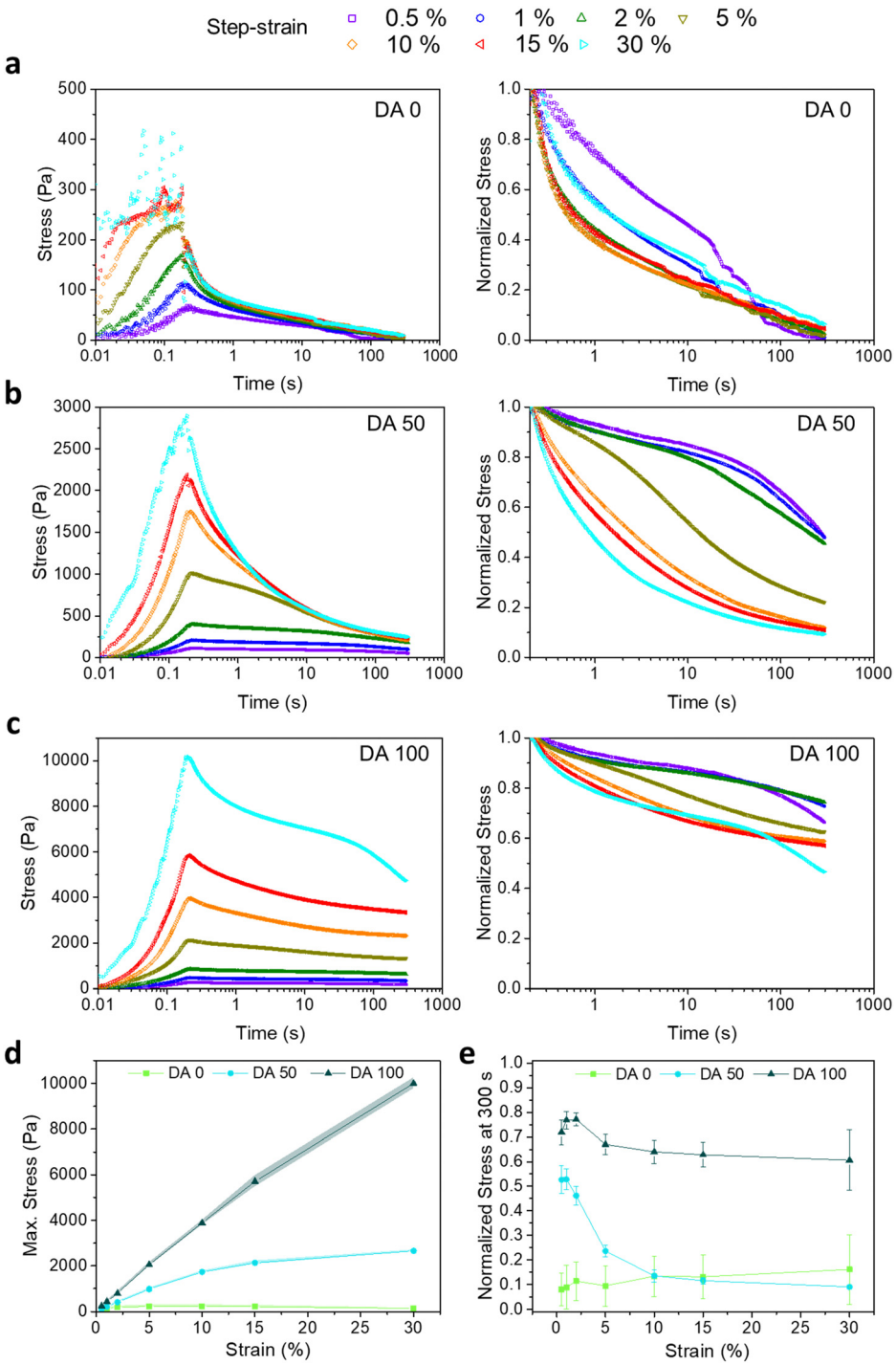


Fig. 2 Representative step-strain stress relaxation curves as a function of increasing applied strain values from 0.5 to 30% on (a) DA 0, (b) DA 50 and (c) DA 100 hydrogels (left) with their corresponding normalized stress values (right, normalized with maximum stress values at 200 ms strain raise time); (d) mean maximum stress values at 200 ms (strain raise time) and (e) normalized stress values at the end of the stress relaxation test (300 s). Error bars indicate standard deviation, $N$ = 2 for DA 0 and DA 50 at 30% applied strain, $N$ = 3 for all the rest.

stress was dissipated faster at higher strains, when the $\gamma_F$ range was reached (Fig. 2e).

The comparative relaxation behavior of DA $X$ hydrogels (for $X$ = 0, 25, 50, 75 and 100) at 1% strain, *i.e.*, within the linear viscoelastic regime, is shown in Fig. 3. The shape of the curves indicates that stress is dissipated by two different relaxations processes with different time scales: a fast first one ($<$1 s) and a slower second one ($>$1 min). To analyze the relaxation mechanisms behind the two processes, the stress relaxation curves were fitted to a linear combination of two stretched exponential

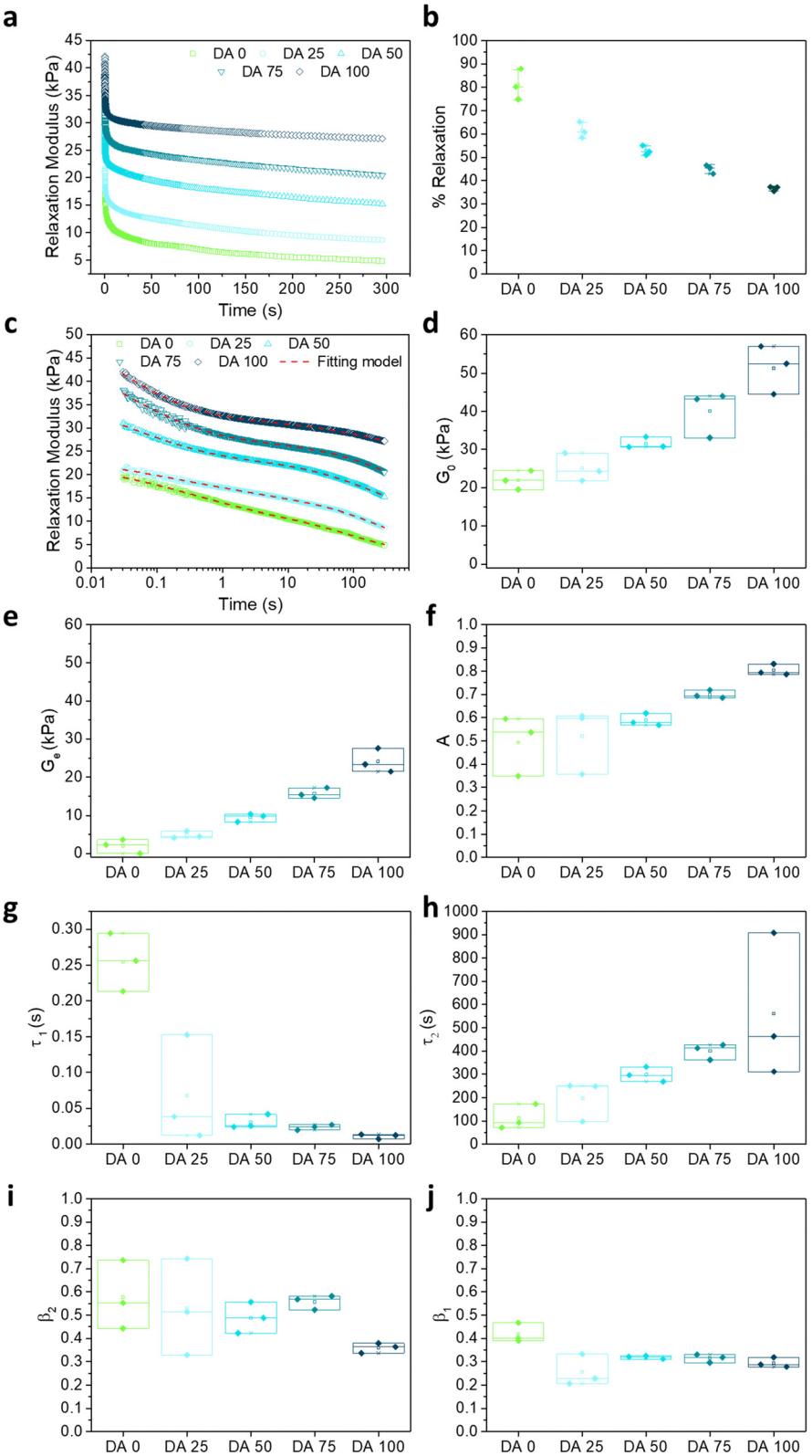


Fig. 3 (a) Representative stress relaxation curves of crosslinked DA *X* hydrogels at a constant applied strain of 1%. (b) Calculated normalized drop of relaxation modulus in DA *X* hydrogels from experiment in (a) at time $t$ = 300 s (see details in experimental section). (c) Stress relaxation curves from (a) represented on a logarithmic scale and the fits to a double stretched exponential function (red dashed lines). Data below 30 ms were not considered for the fitting since this time was required by the equipment to reach a stable strain value of 1%; (d) $G_0$ values as function of *X* that were extrapolated linearly from stress relaxation curves in (a) to time zero. (e)–(j) Fitted parameters as a function of *X*: (e) $G_e$; (f) a (fractional contribution of relaxation 1, fast relaxation process); (g) $\tau_1$; (h) $\tau_2$; (i) $\beta_1$ and (j) $\beta_2$. The experimental curves of three consecutive measurements are shown in Fig. S3 (ESI†). All measurements were performed at room temperature. $N$ = 3, box represents 25 and 75 percentile values and whiskers indicate standard deviation.

 

functions (eqn (1)).[29] The function fitted well with the experimental data with $r^2 > 0.99$ (Fig. 3c). The values of $G_0$, $G_e$, $A$, $\tau_1$, $\tau_2$, $\beta_1$, and $\beta_2$ and are represented in Fig. 3d–j as a function of the hydrogel composition. The two relaxation times $\tau_1$ ($<1$ s) and $\tau_2$ ($>1$ min) differed in more than two orders of magnitude and showed an opposite dependence on the degree of the covalent crosslinking of the hydrogels. $\tau_1$ decreased from 0.25 s to 0.01 s as $X$ increased from 0 to 100 (Fig. 3g), *i.e.* the fast relaxation became faster as the covalent crosslinking degree increased. The relative contribution of this relaxation mode to stress dissipation ($A$ parameter, Fig. 3f) increased with the covalent crosslinking of the hydrogel. The shape parameter $\beta_1$, which reflects the width of the relaxation time distribution, did not show significant changes with the hydrogel composition and is around 0.3–0.4 (Fig. 3g) reflecting a 2–3 decade wide relaxation distribution. The relaxation process at longer time scales became slower in hydrogels with increasing covalent crosslinking (mean $\tau_2$ increased from nearly 100 s to 560 s for DA 0 to DA 100, Fig. 3h) and the strength of this relaxation decreased with $X$. The possible mechanisms behind these relaxations are addressed in the discussion section.

### 3.5. Creep-recovery of DA *X* hydrogels

Fig. 4a shows a creep-recovery experiment with DA $X$ hydrogels at a constant stress of 100 Pa. In DA 25–75 hydrogels an instantaneous deformation was observed, followed by a slower deformation (creep). The instantaneous deformation was more pronounced in hydrogels with higher covalent crosslinking, while the creep process was more pronounced in hydrogels with lower PluDA concentration. DA 100 reached the plateau right after the initial deformation. DA 0 was the farthest from reaching a plateau deformation value during the 180 s of creep. When the 100 Pa stress ceased, an instantaneous and a time-dependent strain recovery was observed for all samples. DA 50–100 almost instantaneously fully recovered to their initial state, which is in agreement with their predominant elastic character as

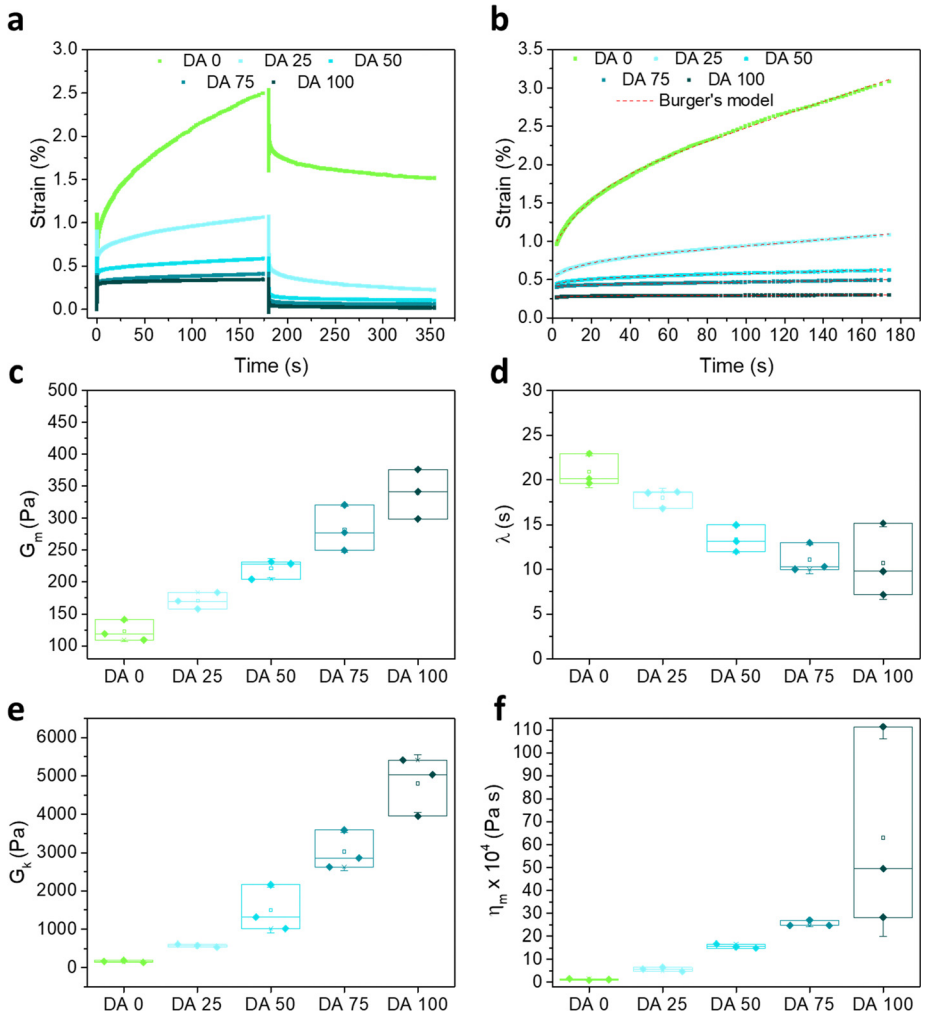


Fig. 4 (a) Representative creep/recovery curves of DA $X$ hydrogels at an applied stress of 100 Pa for 180 s. The strain was monitored during stress application and also during the recovery phase for additional 180 s. Fig. S4 and S5 (ESI†) show all experimental curves. (b) Creep curves and fittings to the Burgers model (eqn (3), red dotted lines), (c)–(f) parameters of the Burgers fitting represented as a function of $X$. $G_m$ and $\eta_m$ denote the spring constant of the spring and the viscosity of the dashpot in the Maxwell element, $G_k$ is the spring constant of the dashpot in the Kelvin element and $\lambda$ is the retardation time. $N$ = 3, box represents 25 and 75 percentile values and whiskers indicate standard deviation.

consequence of the covalent crosslinks. In comparison to that, DA 25 and DA 0 retained a residual deformation (Fig. 4a), in agreement with their predominant physical gel character.

The creep curves were fitted to a four-elements Burgers model (eqn (2))[30–32] (red dashed lines in Fig. 4b), consisting of Maxwell and Kelvin–Voigt elements,[33,38] and obtained fitting parameters as function of the hydrogel composition are represented in Fig. 4c–f. The elastic constants $G_m$ and $G_k$ increased in DA *X* hydrogels with increasing *X*, and therefore an increased elasticity is observed due to a higher number of crosslinks. The reorganization of covalently linked micelles and clusters requires additional work, which causes an increment in the opposition to deformation. This higher resistance capacity contributes to elasticity. In the Burgers model, the retardation time $\lambda$ is connected to the viscoelastic solid material behavior. In the micellar hydrogel model described before, the viscoelastic response is expected to depend on the intermolecular forces between micelles connected by inter-micellar covalent bonds. The shorter retardation times observed with increasing *X* indicate that the covalent connection between the micelles accelerates the sliding of micelles and the deformation of the hydrogel. Furthermore, $\eta_m$ increases with *X* and reflects the increasing dissipative resistance, and thus lesser deformation due to the viscous component. We associate this with sliding of micelles and clusters connected by physical interactions.

The recovery part of the creep experiment was fitted using a Weibull distribution (eqn (3)) equation that is a modification and extension of a simple exponential relaxation. The Weibull equation fitted to the experimental data is shown in Fig. 5a. The delayed viscoelastic strain recovery $\gamma_k$ decreased with increasing covalent crosslinking in DA *X* hydrogels, reflecting that the presence of permanent crosslinks hinders viscoelastic deformation. The permanent irreversible strain $\gamma_p$ was 10 times higher for DA 0 than for the other hydrogels as consequence of the absence of covalent bonds that provide elasticity.

The elastic recovery corresponds to the instantaneous recovered deformation, that is, the Maxwell spring. $\gamma_{maxwell\ spring}$ was calculated as:

$$\gamma_{maxwell\ spring} = \gamma_{ms} = \gamma_{maximum} - (\gamma_k + \gamma_p) \quad (4)$$

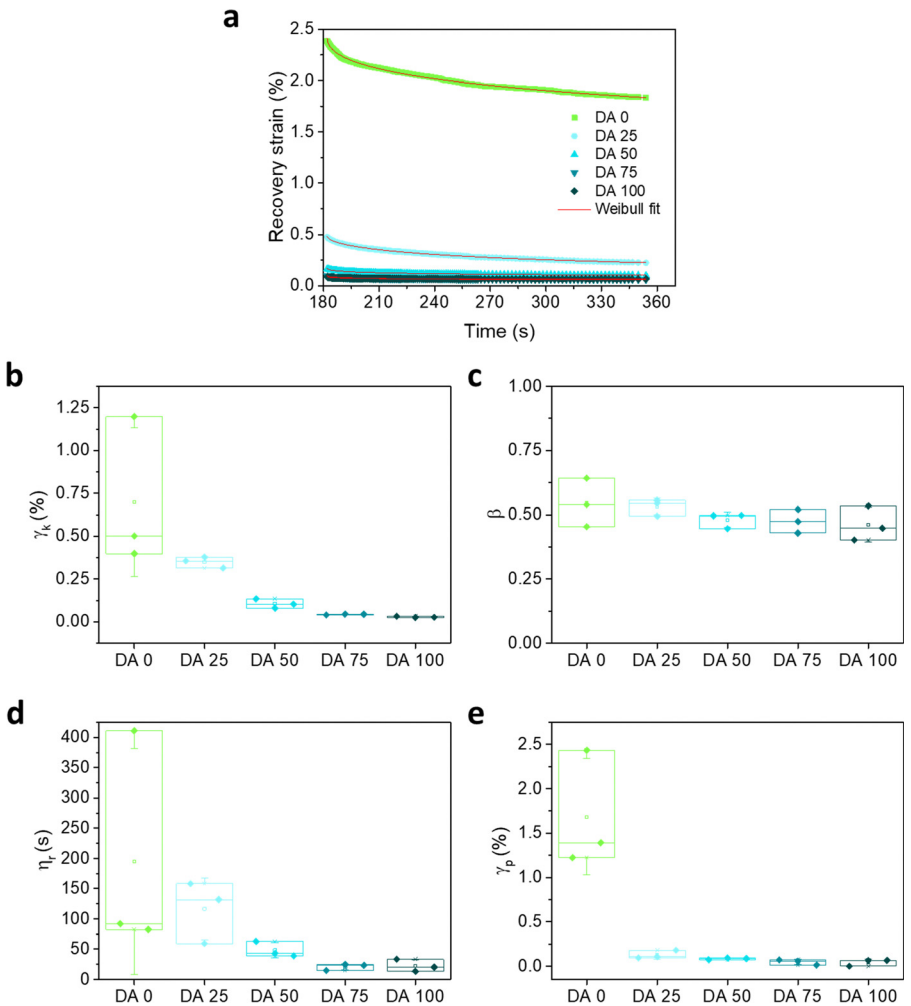


Fig. 5 (a) Recovery curves including fittings to the Weibull distribution function and (b)–(e) parameters of the Weibull fitting as function of DAX composition. *N* = 3, box represents 25 and 75 percentile values and whiskers indicate standard deviation.

 

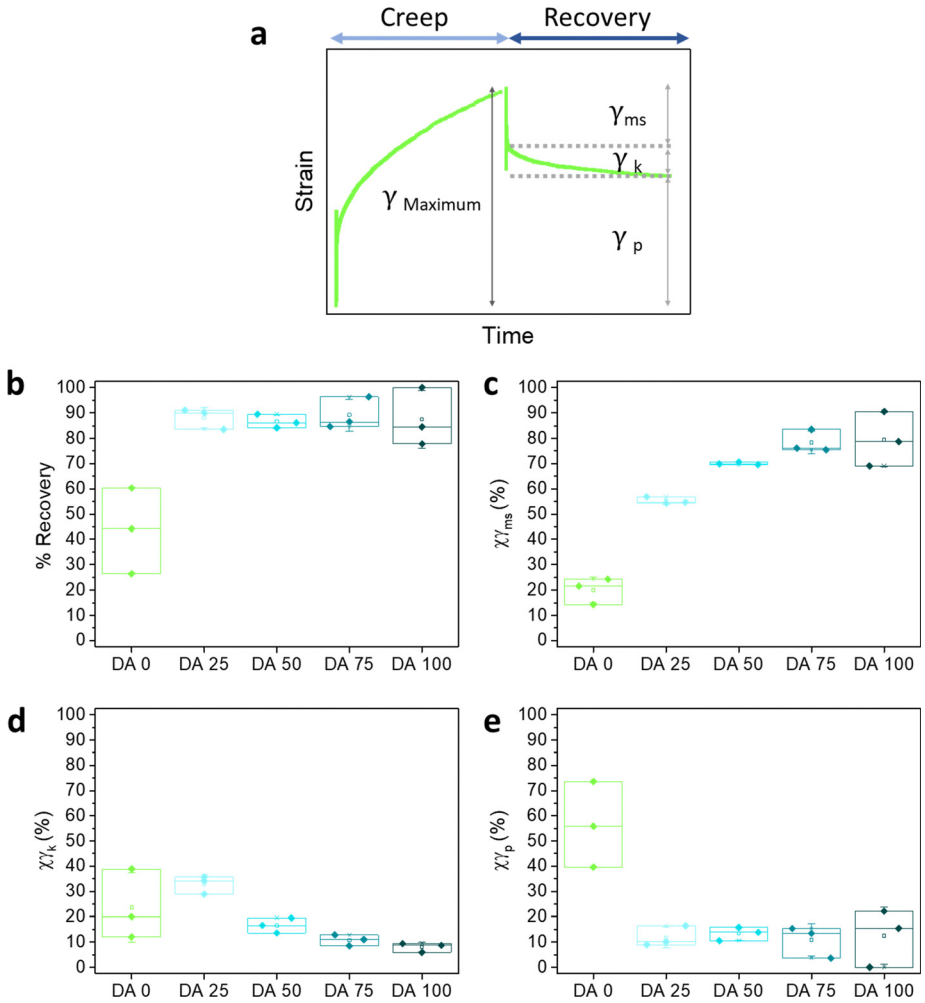


Fig. 6 (a) Elastic, viscoelastic and plastic contributions obtained from the creep-recovery experiment. The curve corresponds to DA 0 at an applied stress of 100 Pa; (b) recovery (%) calculated from recovery curves at 180 s after 100 Pa applied stress; (c)–(e) contributions of elastic, (d) viscoelastic and (e) plastic deformation. $N$ = 3, box represents 25 and 75 percentile values and whiskers indicate standard deviation.

where $\gamma_{maximum}$ is the strain at the end of the creep test. The elastic as well as the viscoelastic and plastic contributions to the deformation extracted from the Weibull model are represented in Fig. 6.[30] At an applied stress of 100 Pa, hydrogels DA 25–100 showed increasing elastic and decreasing viscoelastic responses with increasing covalent crosslinking, and a small plastic response with little dependence on $X$. DA 0 hydrogels showed a strong plastic response and a comparatively much lower elastic and viscoelastic contributions.

## 4. Discussion

The viscoelastic properties of 30 wt% DA $X$ hydrogels can be regulated by adjusting the PluDA fraction in the mixture towards hydrogels of higher elasticity and critical yield strain. The micellar DA $X$ hydrogels are considered granular gels.[39–41] Our rheological observations agree with this picture. In general, the internal structure of granular gels depends on the particle volume fraction and the strength of inter-particle interactions.[42] At high particle volume fractions and weak interaction forces, gelation occurs as a consequence of the dynamical arrest of a phase separation process.[43] In the particle-rich domains, particles aggregate and form clusters that grow until their dynamics is arrested within the 3D network.[44] Clusters act as rigid, load bearing units and have been postulated to be the origin of elasticity in colloidal gel networks. The reversibility of the interactions between particles allows for shear-induced rearrangement of the aggregates and particles by breaking reversible bonds. As a consequence, granular hydrogels show shear thinning behavior. The observed behavior under shear of physical Pluronic hydrogels is in agreement with this picture. The inter-micellar covalent bonds introduced after physical gelation in DA $X$ hydrogels reinforce the stability of the clusters and contribute to a stronger elastic character of the material.[41]

Previous literature discussed the behavior of Pluronic F127 hydrogels under shear.[15,45] Pluronic micelles are considered hard spheres and their regular aggregates can undergo a first order phase transitions (analog melting, recrystallization) or

reorientation as function of shear conditions (shear stress, rate or direction).[15,45] Inter-micellar covalent bonds in DA *X* hydrogels internally stabilize micellar clusters and substantially affect such rearrangement mechanisms and underlying kinetics. We expect that the time scale of these rearrangements relates to the observed experimental time scales for the observed stress relaxation. Our fitting method for the stress relaxation curves of DA *X* hydrogels indicated two different relaxation processes with relaxation times $\tau_1$ (<1 s) and $\tau_2$ (>1 min) that depend on DA content. The fast relaxation process became faster and more prominent with increasing covalent crosslinking. We associate this relaxation to local, structural rearrangements at macroscopic, network scale which require cooperative motion of micelles.[46,47] In contrast, the slow relaxation process could be associated to relaxation modes at microscopic scale, such as the breaking of physical bonds between micelles within clusters, which becomes slower with increasing number of covalent crosslinks.[46,48] A recent article has studied the deformation mechanisms of 24 wt% PluDA hydrogel in an ionic liquid using rheology and SANS.[49] The authors highlighted the possible contribution of free inter-micellar PluDA chains to elasticity by forming covalent inter-micellar bridges. Under tensile stress, the bridging chains would store mechanical energy during stretching and pull micelles back into their original positions after deformation. Although this model could explain our results, the range of stress applied was three orders of magnitude larger than the shear stress applied in our experiments and, therefore, the deformation mechanisms might differ.

DA *X* hydrogels with compositions as studied in this article have been used to encapsulate bacteria (*E. coli*) and to regulate the growth of the embedded bacterial colonies by varying *X*.[1] In Fig. 7 we compare the *X*-dependence of the normalized bacteria colony volume, as obtained in our previous work,[1] with that of the storage modulus (Fig. 1c) and the critical stress for fluidization $\tau_F$ (Fig. S2c, ESI†). A decrease in the colony volume and an increase of $G'$ and $\tau_F$ with *X* was observed in DA 0–75 hydrogels. The colony volume in DA 100 is similar as in DA 75, suggesting that the mechanical differences between these two hydrogels are out of the mechanosensing capacity of the bacteria colonies. The elastic contribution to deformation $X\gamma_{ms}$ (Fig. 6c) in our creep-recovery experiments was similar for DA 75 and DA 100 and correlated inversely with the trend of colony volume, suggesting that this could also be a relevant mechanical parameter to predict bacteria behavior inside the hydrogels with higher PluDA fraction.

Bacteria exert forces on the surrounding matrix while growing as consequence of their internal turgor pressure (Fig. 8). This turgor pressure is characteristic for the bacteria species and is ranged between 30 and 300 kPa for *E. coli*.[50] The growth rate of *E. coli* in suspension and in the presence of nutrients is >20 minutes. According to our rheological results (Fig. 1a and Fig. S2, ESI†), a hypothetical stress of 10 kPa at a time scale of 20 minutes applied by growing *E. coli* to a surrounding DA *X* matrix would deform the hydrogel beyond the yield point. Therefore, the observed correlation in our studies between

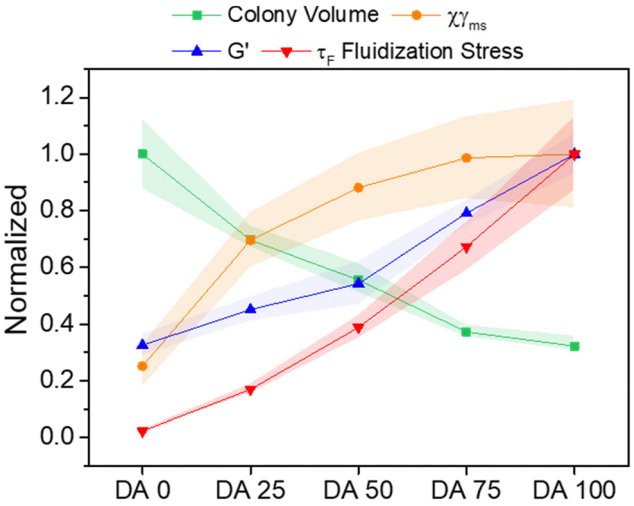


Fig. 7 Comparative plot of normalized mechanical parameters from this article and bacteria growth volume as function of DA *X* composition from.[1] The represented normalized parameters are: colony volume (95th percentile volumes of colonies after 24 h growth), the elastic contribution to deformation $X\gamma_{ms}$ (maxwell spring) in creep-recovery experiments (applied stress of 100 Pa), shear storage modulus $G'$ (at 1 Hz) and Fluidization stress $\tau_F$. The values were normalized with respect to the highest value in each category. The symbols and shaded regions of the normalized colony volume data indicate 95 ± 2 percentile value range, for all other data the symbols and shaded regions indicate mean ± SD.

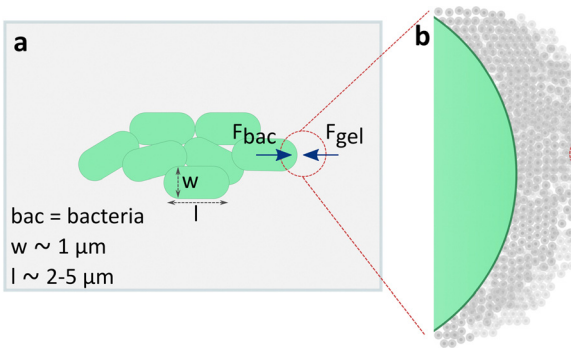


Fig. 8 Representation of a growing bacteria colony embedded in DA *X* hydrogel.

colony volume and the fluidization stress seems reasonable as a first interpretation. Additional studies and multiparametric models are needed to understand the underlying principles behind the dependence of bacteria growth and the mechanical properties of the confining space.

## Conclusions

The presented results describe the rheological behavior of Plu/PluDA hydrogels with compositions relevant for embedding and culturing bacteria. This fundamental study can support current and future work with Pluronic-based hydrogels in technologies that use encapsulated bacteria, like in ELM development or in biotechnological production in immobilized cell

 

reactors. Mechanical confinement of an expanding bacterial colony and the mechanical resistance of the environment to the colony growth are also proven to be important factors in triggering biofilm development, also in infection scenarios. Future understanding of the correlation between the material mechanical parameters in DA *X* hydrogels and the cell responses in these model encapsulated systems can also help to understand the natural cases.

## Data availability statement

The raw/processed data required to reproduce these findings cannot be shared at this time due to technical or time limitations.

## Author contributions

Shardul Bhusari: conceptualization, methodology, validation, visualization, formal analysis, investigation, writing – original draft. Maxi Hoffmann: validation, writing – review & editing. Petra Herbeck-Engel: investigation (Raman experiments). Shrikrishnan Sankaran: writing – review & editing. Manfred Wilhelm: writing – review & editing. Aránzazu del Campo: conceptualization, supervision, validation, writing – original draft, writing – review & editing, funding acquisition.

## Conflicts of interest

The authors declare that they have no known competing financial interests or personal relationships that could have appeared to influence the work reported in this paper.

## Acknowledgements

The authors acknowledge support from the Deutsche Forschungsgemeinschaft (Collaborative Research Centre, SFB 1027) and the Leibniz Science Campus Living Therapeutic Materials, LifeMat. The authors thank Lea Fischer for providing feedback to the manuscript.

## References

1 S. Bhusari, S. Sankaran and A. del Campo, Regulating bacterial behavior within hydrogels of tunable viscoelasticity, *Adv. Sci.*, 2022, **9**(17), 2106026.
2 M. Rizwan, A. E. G. Baker and M. S. Shoichet, Designing Hydrogels for 3D Cell Culture Using Dynamic Covalent Crosslinking, *Adv. Healthcare Mater.*, 2021, **10**(12), 2100234.
3 X. Liu, M. E. Inda, Y. Lai, T. K. Lu and X. Zhao, Engineered Living Hydrogels, *Adv. Mater.*, 2022, **34**(26), 1–22.
4 D. Indana, P. Agarwal, N. Bhutani and O. Chaudhuri, Viscoelasticity and Adhesion Signaling in Biomaterials Control Human Pluripotent Stem Cell Morphogenesis in 3D Culture, *Adv. Mater.*, 2021, **33**(43), 2101966.
5 A. K. Yanamandra, S. Bhusari, A. del Campo, S. Sankaran and B. Qu, In vitro evaluation of immune responses to bacterial hydrogels for the development of living therapeutic materials, *Biomater. Adv.*, 2023, **153**, 213554.
6 X. Liu, H. Yuk, S. Lin, G. A. Parada, T. C. Tang and E. Tham, *et al.*, 3D Printing of Living Responsive Materials and Devices, *Adv. Mater.*, 2018, **30**(4), 1704821.
7 T. G. Johnston, S. F. Yuan, J. M. Wagner, X. Yi, A. Saha and P. Smith, *et al.*, Compartmentalized microbes and co-cultures in hydrogels for on-demand bioproduction and preservation, *Nat. Commun.*, 2020, **11**(1), 563.
8 T. Butelmann, H. Priks, Z. Parent, T. G. Johnston, T. Tamm and A. Nelson, *et al.*, Metabolism Control in 3D-Printed Living Materials Improves Fermentation, *ACS Appl. Bio Mater.*, 2021, **4**, 7195–7203.
9 A. Saha, T. G. Johnston, R. T. Shafranek, C. J. Goodman, J. G. Zalatan and D. W. Storti, *et al.*, Additive Manufacturing of Catalytically Active Living Materials, *ACS Appl. Mater. Interfaces*, 2018, **10**(16), 13373.
10 D. Attwood, J. H. Collett and C. J. Tait, The micellar properties of the poly(oxyethylene) - poly(oxypropylene) copolymer Pluronic F127 in water and electrolyte solution, *Int. J. Pharm.*, 1985, **26**(1–2), 25–33.
11 M. Di Biase, P. De Leonardis, V. Castelletto, I. W. Hamley, B. Derby and N. Tirelli, Photopolymerization of Pluronic F127 diacrylate: A colloid-templated polymerization, *Soft Matter*, 2011, **7**(10), 4928.
12 R. Basak and R. Bandyopadhyay, Encapsulation of hydrophobic drugs in pluronic F127 micelles: Effects of drug hydrophobicity, solution temperature, and pH, *Langmuir*, 2013, **29**(13), 4350.
13 P. Prasanthan and N. Kishore, Self-assemblies of pluronic micelles in partitioning of anticancer drugs and effectiveness of this system towards target protein, *RSC Adv.*, 2021, **11**(36), 22057.
14 Q. Gao, Q. Liang, F. Yu, J. Xu, Q. Zhao and B. Sun, Synthesis and characterization of novel amphiphilic copolymer stearic acid-coupled F127 nanoparticles for nano-technology based drug delivery system, *Colloids Surf., B*, 2011, **88**(2), 741.
15 J. Jiang, C. Burger, C. Li, J. Li, M. Y. Lin and R. H. Colby, *et al.*, Shear-induced layered structure of polymeric micelles by SANS, *Macromolecules*, 2007, **40**(11), 4016.
16 P. Alexandridis and T. Alan Hatton, Poly(ethylene oxide)poly(propylene oxide)poly(ethylene oxide) block copolymer surfactants in aqueous solutions and at interfaces: thermodynamics, structure, dynamics, and modeling, *Colloids Surf., A*, 1995, **96**(1–2), 1–46.
17 J. Goodwin and R. Hughes, *Rheology for chemists: An Introduction*, Royal Society of Chemistry, 2008.
18 K. Hyun, J. G. Nam, M. Wilhellm, K. H. Ahn and S. J. Lee, Large amplitude oscillatory shear behavior of PEO-PPO-PEO triblock copolymer solutions, *Rheol. Acta*, 2006, **45**(3), 239.
19 S. C. Millik, A. M. Dostie, D. G. Karis, P. T. Smith, M. McKenna and N. Chan, *et al.*, 3D printed coaxial nozzles for the extrusion of hydrogel tubes toward modeling vascular endothelium, *Biofabrication*, 2019, **11**(4), 045009.

20 W. Zhang, Y. Shi, Y. Chen, J. Ye, X. Sha and X. Fang, Biomaterials Multifunctional Pluronic P123/F127 mixed polymeric micelles loaded with paclitaxel for the treatment of multidrug resistant tumors, *Biomaterials*, 2011, **32**(11), 2894.
21 C. J. Wu, A. K. Gaharwar, B. K. Chan and G. Schmidt, Mechanically tough Pluronic F127/Laponite® nanocomposite hydrogels from covalently and physically cross-linked networks, *Macromolecules*, 2011, **44**(20), 8215.
22 S. Bhusari, J. Kim, K. Polizzi, S. Sankaran and A. del Campo, Encapsulation of bacteria in bilayer Pluronic thin film hydrogels: A safe format for engineered living materials, *Biomater. Adv.*, 2023, **145**, 213240.
23 H. Priks, T. Butelmann, A. Illarionov, T. G. Johnston, C. Fellin and T. Tamm, *et al.*, Physical Confinement Impacts Cellular Phenotypes within Living Materials, *ACS Appl. Bio Mater.*, 2020, **3**(7), 4273.
24 M. Lufton, O. Bustan, B. Hen Eylon, E. Shtifman-Segal, T. Croitoru-Sadger and A. Shagan, *et al.*, Living Bacteria in Thermoresponsive Gel for Treating Fungal Infections, *Adv. Funct. Mater.*, 2018, **28**(40), 1801581.
25 M. Müller, J. Becher, M. Schnabelrauch and M. Zenobi-Wong, Nanostructured Pluronic hydrogels as bioinks for 3D bioprinting, *Biofabrication*, 2015, **7**(3), 035006.
26 P. Bertsch, L. Andrée, N. H. Besheli and S. C. G. Leeuwenburgh, Colloidal hydrogels made of gelatin nanoparticles exhibit fast stress relaxation at strains relevant for cell activity, *Acta Biomater.*, 2022, **138**, 124.
27 M. Dinkgreve, J. Paredes, M. M. Denn and D. Bonn, On different ways of measuring "the" yield stress, *J. Non-Newtonian Fluid Mech.*, 2016, **238**, 233.
28 M. Zabet, S. Mishra and S. Kundu, Effect of graphene on the self-assembly and rheological behavior of a triblock copolymer gel, *RSC Adv.*, 2015, **5**(102), 83936.
29 T. Iyo, Y. Maki, N. Sasaki and M. Nakata, Anisotropic viscoelastic properties of cortical bone, *J. Biomech.*, 2004, **37**(9), 1433.
30 Y. Jia, K. Peng, X. L. Gong and Z. Zhang, Creep and recovery of polypropylene/carbon nanotube composites, *Int. J. Plast.*, 2011, **27**(8), 1239.
31 S. Nam, J. Lee, D. G. Brownfield and O. Chaudhuri, Viscoplasticity Enables Mechanical Remodeling of Matrix by Cells, *Biophys. J.*, 2016, **111**(10), 2296.
32 X. Hong, J. P. Stegemann and C. X. Deng, Microscale characterization of the viscoelastic properties of hydrogel biomaterials using dual-mode ultrasound elastography, *Biomaterials*, 2016, **88**, 12–24.
33 H. L. Ornaghi, J. H. S. Almeida, F. M. Monticeli and R. M. Neves, Stress relaxation, creep, and recovery of carbon fiber non-crimp fabric composites, *Compos., Part C: Open Access*, 2020, **3**, 100051.
34 T. H. Qazi, V. G. Muir and J. A. Burdick, Methods to Characterize Granular Hydrogel Rheological Properties, Porosity, and Cell Invasion, *ACS Biomater. Sci. Eng.*, 2022, **8**(4), 1427.
35 E. Dickinson, Structure and rheology of colloidal particle gels: Insight from computer simulation, *Adv. Colloid Interface Sci.*, 2013, **199–200**, 114.
36 G. J. Donley, P. K. Singh, A. Shetty and S. A. Rogers, Elucidating the G'' overshoot in soft materials with a yield transition via a time-resolved experimental strain decomposition, *Proc. Natl. Acad. Sci. U. S. A.*, 2020, **117**(36), 21945.
37 M. Malmeten and B. Lindman, Self-Assembly in Aqueous Block Copolymer Solutions, *Macromolecules*, 1992, **25**, 5440.
38 K. S. Fancey, A mechanical model for creep, recovery and stress relaxation in polymeric materials, *J. Mater. Sci.*, 2005, **40**(18), 4827.
39 B. Shriky, A. Kelly, M. Isreb, M. Babenko, N. Mahmoudi and S. Rogers, *et al.*, Pluronic F127 thermosensitive injectable smart hydrogels for controlled drug delivery system development, *J. Colloid Interface Sci.*, 2020, **565**, 119.
40 H. Tsurusawa, M. Leocmach, J. Russo and H. Tanaka, Direct link between mechanical stability in gels and percolation of isostatic particles, *Sci. Adv.*, 2019, **5**(5), 1–8.
41 L. C. Hsiao, R. S. Newman, S. C. Glotzer and M. J. Solomon, Role of isostaticity and load-bearing microstructure in the elasticity of yielded colloidal gels, *Proc. Natl. Acad. Sci. U. S. A.*, 2012, **109**(40), 16029.
42 M. Y. Lin, H. M. Lindsay, D. A. Weitz, R. C. Ball, R. Klein and P. Meakin, Universality in colloid aggregation, *Nature*, 1989, **339**(6223), 360.
43 H. Tsurusawa, S. Arai and H. Tanaka, A unique route of colloidal phase separation yields stress-free gels, *Sci. Adv.*, 2020, **6**(41), 1–11.
44 K. A. Whitaker, Z. Varga, L. C. Hsiao, M. J. Solomon, J. W. Swan and E. M. Furst, Colloidal gel elasticity arises from the packing of locally glassy clusters, *Nat. Commun.*, 2019, **10**(1), 2237.
45 C. R. López-Barrón, N. J. Wagner and L. Porcar, Layering, melting, and recrystallization of a close-packed micellar crystal under steady and large-amplitude oscillatory shear flows, *J. Rheol.*, 2015, **59**(3), 793–820.
46 B. Nyström, H. Walderhaug and F. K. Hansen, Dynamic light scattering and rheological studies of thermoreversible gelation of a poly(ethylene oxide)-poly(propylene oxide)-poly(ethylene oxide) triblock copolymer in aqueous solution, *Faraday Discuss.*, 1995, **101**, 335.
47 L. Mohan, M. Cloitre and R. T. Bonnecaze, Build-up and two-step relaxation of internal stress in jammed suspensions, *J. Rheol.*, 2015, **59**(1), 63–84.
48 T. Murakami, T. Kawamori, J. D. Gopez, A. J. McGrath, D. Klinger and K. Saito, Synthesis of PEO-based physical gels with tunable viscoelastic properties, *J. Polym. Sci., Part A: Polym. Chem.*, 2018, **56**(10), 1033.
49 C. R. Lopez-Barron, R. Chen, N. J. Wagner and P. J. Beltramo, Self-Assembly of Pluronic F127 Diacrylate in Ethylammonium Nitrate: Structure, Rheology, and Ionic Conductivity before and after Photo-Cross-Linking, *Macromolecules*, 2016, **49**, 5179.
50 M. Osawa and H. P. Erickson, Turgor pressure and possible constriction mechanisms in bacterial division, *Front. Microbiol.*, 2018, **9**, 1–7.

 